强激光与粒子束
High Power Laser and Particle Beams

1.3 GHz连续波超导射频腔的数字低电平射频系统和腔模拟器设计及测试

刘奎　王程　黄宇轩　朱坤托　王滔

Digital low-level radio frequency system and cavity simulator for 1.3 GHz continuous-wave superconducting radio-frequency cavity

Liu Kui, Wang Cheng, Huang Yuxuan, Zhu Kuntuo, Wang Tao

引用本文:
刘奎, 王程, 黄宇轩, 朱坤托, 王滔. 1.3 GHz连续波超导射频腔的数字低电平射频系统和腔模拟器设计及测试[J]. 强激光与粒子束, 2024, 36: 084005. doi: 10.11884/HPLPB202436.230325
Liu Kui, Wang Cheng, Huang Yuxuan, Zhu Kuntuo, Wang Tao. Digital low-level radio frequency system and cavity simulator for 1.3 GHz continuous-wave superconducting radio-frequency cavity[J]. *High Power Laser and Particle Beams*, 2024, 36: 084005. doi: 10.11884/HPLPB202436.230325

在线阅读 View online: https://doi.org/10.11884/HPLPB202436.230325

第 36 卷第 8 期
2024 年 8 月

强 激 光 与 粒 子 束
HIGH POWER LASER AND PARTICLE BEAMS

Vol. 36，No. 8
Aug.，2024

·Particle Beams and Accelerator Technology·

Digital low-level radio frequency system and cavity simulator for 1.3 GHz continuous-wave superconducting radio-frequency cavity*

Liu Kui[1,2]， Wang Cheng[3]， Huang Yuxuan[1,2]， Zhu Kuntuo[1,2]， Wang Tao[1,2]

（1. *Key Laboratory of Intelligent Computing Technology*, *SAST*, *Shanghai* 201109, *China*;
2. *Shanghai Aerospace Electronic Technology Institute*, *Shanghai* 201109, *China*;
3. *Shanghai Advanced Research Institute*, *Chinese Academy of Sciences*, *Shanghai* 201210, *China*）

Abstract: A highly precise low-level radio-frequency (LLRF) system for a 1.3 GHz continuous-wave (CW) superconducting radio-frequency (RF) cavity is required to stabilize the electromagnetic field of cavities. However, because of the high loaded quality factor and wide electromagnetic frequency band of the 1.3 GHz CW RF cavity, the RF cavity has a small electromagnetic bandwidth in the frequency domain. The small electromagnetic frequency mismatch between the RF power source and RF cavity can easily cause ponderomotive instabilities in the generator driven resonator control system, eventually resulting in variations in the electromagnetic field of the cavity. In this study, a self-excited loop (SEL) control system was developed to prevent the occurrence of ponderomotive instabilities and compensate for the effects of microphonics noise. In addition, a digital 1.3 GHz RF cavity simulator, which can easily verify the designed algorithms of the LLRF system, was developed. The recorded measurements show that the SEL control system can ensure stability of the cavity field even when the RF cavity is detuned by 5 Hz. The comparison and validation have verified that the cavity simulator is a reliable platform to test the new algorithms.

Key words: RF cavity simulator, self-excited loop, generator driven resonator, low-level RF system

CLC number: TL506 **Document code:** A **doi**: 10.11884/HPLPB202436.230325

The Shanghai high repetition rate X-ray free electron laser and extreme light facility (SHINE) provides ultra-short and high lightness coherent X-ray pulses with the wavelengths less than 0.1 nm. It's a gigantic super-microscope that even can be used to observe the movements of the atoms during the chemical reactions. Because of these characteristics, the hard X-ray free electron laser has a great improvement to the development of materials physics, chemistry, biochemistry, structural biology, plasma physics, etc[1-2].To obtain the ultrashort X-ray pulses for observing fast movement, the high repetition rate of electron bunches is necessary. As the traditional pulse-operated radiofrequency (RF) cavity can not be qualified to this work, the SHINE is operated at repetition rate of 1 MHz and is driven by a 1.3 GHz continuous-wave (CW) superconducting linac[3-4].

For 1.3 GHz CW-operated radio-frequency (RF) cavities, the high loaded quality factor (about 10^7) and ultra high frequency (UHF) band lead to an extremely narrow electromagnetic bandwidth. A small detuning frequency of the RF cavity results in a sizable change in the amplitude and phase of the cavity field. The steady Lorentz force detuning can be easily compensated for by pre-detuning the cavities over a mechanical tuner; however, mechanical microphonic noise of the cavities is difficult to remove[5]. In this study, a digital low-level radio-frequency (LLRF) control system with a generator driven resonant (GDR) mode and a self-excited loop (SEL) mode was developed to operate the RF cavity and avoid the occurrence of ponderomotive instabilities. The locked SEL could also be used to compensate for the effects of microphonics noise. In addition, an RF cavity simulator was developed and implemented on digital hardware.

1 Principle behind LLRF control system

For CW-operated TESLA cavity, there are many detuning sources than will detune the cavity, such as Lorentz force

* **Received date:** 2023-09-19; **Revised date:** 2024-04-15
E-mail: Liu Kui, liukui_804@163.com。

detuning (LFD) due to large electromagnetic field and the wall current. The LFD incorporates in several mechanical eigenmodes, as well as couples external mechanical noises. The second order model of dynamic LFD in time domain is given by

$$\Delta\ddot{\omega}_k(t)+\frac{2}{\tau_k}\Delta\dot{\omega}_k(t)+\Omega_k^2\Delta\omega_k(t)=-2\Omega_k^2K_kV_0^2\Delta V(t) \tag{1}$$

where $\Delta\omega_k(t)$ is frequency shift of the electromagnetic that contribute by mechanical mode k, τ_k is the damping time constant of each mode, Ω_k is the eigenfrequecy of mechanical mode k, K_k is lorentz force coefficient, and $\Delta V(t)$ is the variation of cavity field voltage. From the research of Neumann[6], the steady LFD is easy to be compensated by pre-detune of the cavities over mechanical tuner. And LFD also occurs less after the feedback suppresses to field amplitude.

For CW-operated TESLA cavity, the major error sources are the mechanical microphonics of the cavity, for example, helium pressure fluctuations, vibrations of vacuum pump and water cooling pump, and “random” broadband machinery noise[7]. The influences of microphonics not only cause the phase shift of cavity field, but also are amplified by dynamic Lorentz force detuning Eq.(1), resulting in the large variations of amplitude of cavity field. In RF feedback loop, this can lead to ponderomotive instabilities.

Ponderomotive instabilities consist of monotonic instability and oscillatory instability. The monotonic instability is a phenomenon that amplitude drop of cavity electromagnetic field increase or decrease exponentially until limited by nonlinear effects. The oscillatory instability comes from the interaction between cavity electronmagnetic field and LFD effect and also oscillated at an exponential rate until limited by nonlinear effects[8-9].

The LLRF control system has three main types of control systems. The first is the GDR control system, whose resonator is driven by an external RF reference and is modulated by the control system. For simplification, only one type of amplitude and phase feedback control system is presented in Fig.1. The GDR system is best suited for a low-loaded quality factor cavity in the pulsed operation when the cavity is resonant or has a low detuning frequency. The system exhibits a fast and predictable rise time and good performance in vector sum control; however, its power up may be easily hampered because of the ponderomotive instabilities[10].

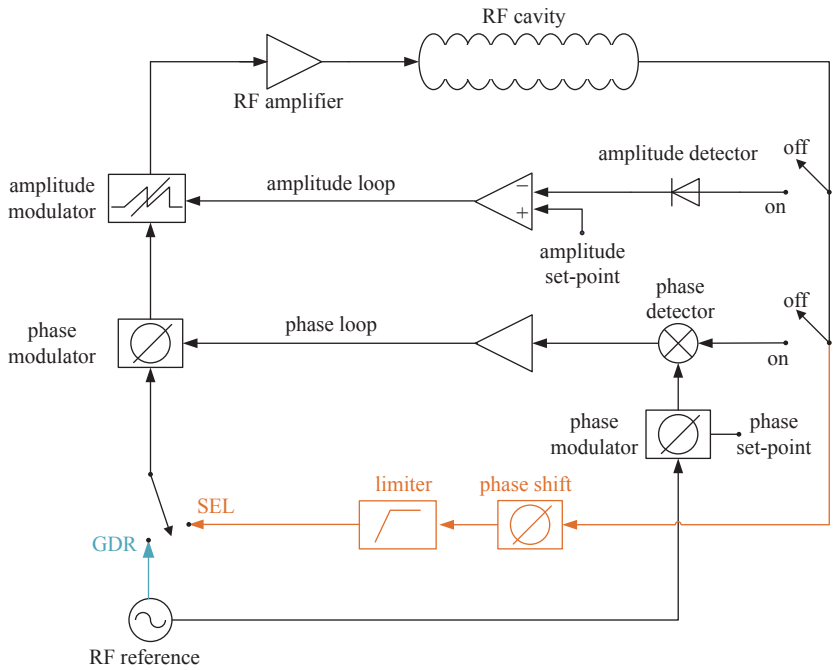

Fig. 1 Simplified diagram of the GDR and SEL system

The second is the SEL system, which was first presented as an analog form by Delayen[11]. As shown in Fig.1, SEL uses an RF cavity, phase shifter, limiter, and amplifier to form an oscillator loop; this is called a free SEL. These elements ensure that the loop gain is larger than 1, the loop phase is a multiple of 2π, the amplitude is limited, and the loop oscillates constantly.

Eventually, the frequency of the SEL loop can be used to track the frequency of the RF cavity in real time, even if the cavity has detuned many bandwidths. Once the loop oscillates, the amplitude of the RF cavity can be locked to a set point after switching on the amplitude feedback loop. When the frequency of the RF cavity is sufficiently close to the resonant frequency after tuning using the mechanical tuning system and if the phase feedback loop is turned on, the SEL would practically resemble a phase-locked loop (PLL) system, and the frequency of the loop would be locked to the reference frequency[12]. This is referred to as locked SEL. Such an SEL is suited for high gradient, high loaded quality factor, and very narrow bandwidth cavities that operate in the CW mode. It can push the ponderomotive instabilities arbitrarily far using amplitude feedback and is unaffected by Lorentz detuning at power up[13].

The third is the PLL system, Jefferson Lab's research found that while PLL system can also track the resonant frequency of a continuous-wave cavity, SEL systems is easier to follow in real time and arbitrarily adjust the gradient and even phase of the cavity field. And, the SEL system is more effective at mitigating microphone noise in the superconducting cavity[14].

2 Digital LLRF control system for 1.3 GHz CW RF cavity

The electromagnetic frequency band of the 1.3 GHz RF cavity is very high. Thus, it cannot be directly sampled by an analog-to-digital converter (ADC). In the LLRF system, the down-conversion technique is adopted by an analog front-end, which mixes the RF signal with a local oscillator (LO) signal and then removes the high-frequency part using an analog low-pass filter. Then, an intermediate frequency (IF) signal is obtained. The local oscillator generator module (LOGM) receives an input of 1 300 MHz RF signal from a master oscillator and provides a 1 300 MHz reference signal (REF), 1 354 MHz LO signal, 81.25 MHz clock to micro rear transition module (mRTM), and an advanced mezzanine card (AMC) board. The mRTM is mostly used as an analog front-end for the AMC and is responsible for the down-conversion and up-conversion of RF signals. The AMC usually includes the digital part including a field programmable gate array (FPGA) chip, ADC, digital to analog converter (DAC), and data planes. The zone connector is used to connect the mRTM with the AMC. Because of the separated design of the digital parts and analog front-end parts, the module can be easily upgraded. On some advanced AMC boards, the central processing unit (CPU), graphics processing unit (GPU), and solid state disk (SSD) can be integrated into the boards[15].

A schematic diagram of the LLRF framework is presented in Fig.2. On the mRTM card, the RF signal from the cavity field is down-converted to IF, then is attenuated, and transferred to the ADC on the AMC card via zone 3. The up-conversion process is also completed on the mRTM card. On the AMC card, the LLRF algorithms mainly run on the FPGA. The non-IQ technique can demodulate the IF to the in-phase (I) and quadrature (Q) signals and can use the coordinate rotation digital computer (CORDIC) algorithm to convert the IQ to amplitude and phase signals. Then, the signals are processed by the SEL and GDR control algorithm and are converted to IQ from the amplitude and phase by CORDIC. The hexagonal box presents an additional phase feedback loop in the IQ loop, which is developed to compensate for the effects of microphonics.

In the modern ADC of the digital LLRF system, a small differential nonlinearity will generate high harmonics of the input carrier[16]. However, the non-IQ technique can ensure most alias harmonics remain out of the baseband signal by slightly

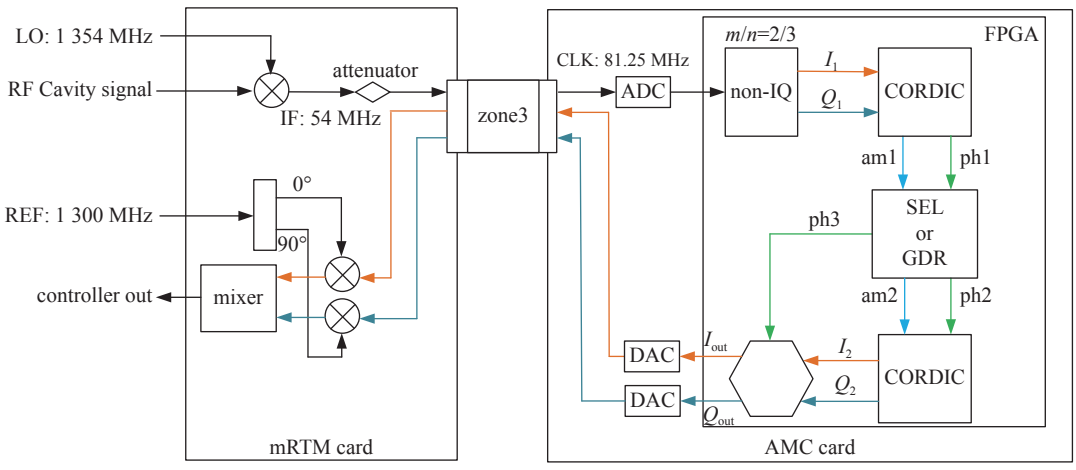

Fig. 2 Schematic diagram of LLRF system framework

changing the sampling rate. Assuming that m and n are integers corresponding to sampling m IF periods with n samples. The sampling rate can be described as:

$$\frac{n}{m}=\frac{f_{\mathrm{clk}}}{f_{\mathrm{IF}}}=\frac{2\pi}{\Delta\varphi} \tag{2}$$

where, $\Delta\varphi$ is the phase advance between two consecutive ADC samples. In this study, the LLRF system applies $m=2$ and $n=3$.

The non-IQ algorithm calculates the in-phase and quadrature components of the envelope vector of IF signals based on the last n samples by[17]

$$\begin{cases} I_i=\dfrac{2}{n}\displaystyle\sum_{k=i-n+1}^{i} y_k\sin(k\Delta\varphi) \\ Q_i=\dfrac{2}{n}\displaystyle\sum_{k=i-n+1}^{i} y_k\cos(k\Delta\varphi) \end{cases} \tag{3}$$

where y_k is the kth ADC sample of the IF signal. In the digital LLRF system, the non-IQ algorithm can be easily implemented with a moving-average finite impulse response (FIR) filter and the coefficients exist as a look-up table.

The IQ, amplitude, and phase can be transformed to each other by the CORDIC algorithm in the digital system. In addition, the transformation needs to be rapid, precise, and continuous for perfectly realizing the function of the SEL. To the accuracy of the CORDIC algorithm, the phase error is more evident than amplitude error, but it can still be less than 0.05% after 18 iterations in theory[18,19] provide an iterative method of vector rotation to calculate the transcendental function by arbitrary angles using only shifts, multipliers, and adds in Eq.(4).

$$\begin{cases} x_{i+1}=K_i[x_i-y_i d_i 2^{-i}] \\ y_{i+1}=K_i[y_i+x_i d_i 2^{-i}] \\ \mathrm{z}_{i+1}=\mathrm{z}_i-d_i\arctan(2^{-i}) \end{cases} \tag{4}$$

where $K_i=1/\sqrt{1+2^{-2i}}$, $d_i=\pm1$. The CORDIC algorithm is limited to rotation angles between $[-\pi/2,\pi/2]$ due to the use of 2^0 for the tangent in the first iteration. To meet the function of the SEL control system, the sign of IQ value also need be considered and added into the CORDIC algorithm to expand the rotation angles to $[-\pi,\pi]$. Moreover, the inherent CORDIC block of the system generator can not process large and rapidly changing loop phase. In the future, a new CORDIC block which can overcome this disadvantage will be developed to substitute the old one.

To satisfy the high requirements of the modern digital LLRF system, micro telecommunications computing architecture (MicroTCA.4) was developed to afford a high measurement precision, low latency, parallel processing, compact standard, high reliability, and availability of a digital system. Its essential parts include a crate with a backplane, a power supply module (PM), a cooling unit (CU), a MicroTCA carrier hub (MCH), an AMC, and an mRTM[14]. In this study, the LLRF system was developed and implemented based on MicroTCA.4 at the digital lab of the MSK group in Deutsches Elektronen-Synchrotron (DESY).

A. Structures of SEL and GDR control system

The structures of the SEL and GDR systems are presented in Fig.3. The 54 MHz IF signals first were sampled using a 81.25 MHz sampling frequency; the signals then went through the non-IQ block and CORDIC module, and were transferred to amplitude and phase signals. The multiplexers were chosen to expediently switchover the following three modes.

In the GDR mode, proportional-integral-derivative (PID) controllers are used in amplitude and phase feedback loops. Practically, the LLRF control system only uses a proportional-integral (PI) controller; the PI can be adjusted to obtain an open-loop system. The GDR mode is basically fit for operating in the resonant frequency that is highly close to the RF reference frequency.

In the free SEL mode, the SEL loop can obtain positive feedback by appropriate adjustment of the shifter. The amplitude loop can switch to the amplitude set-point or the PID feedback loop to achieve a value which is closer to the amplitude set point. Using the SEL mode, the system can rapidly track the cavity frequency even when the cavity is detuned by many

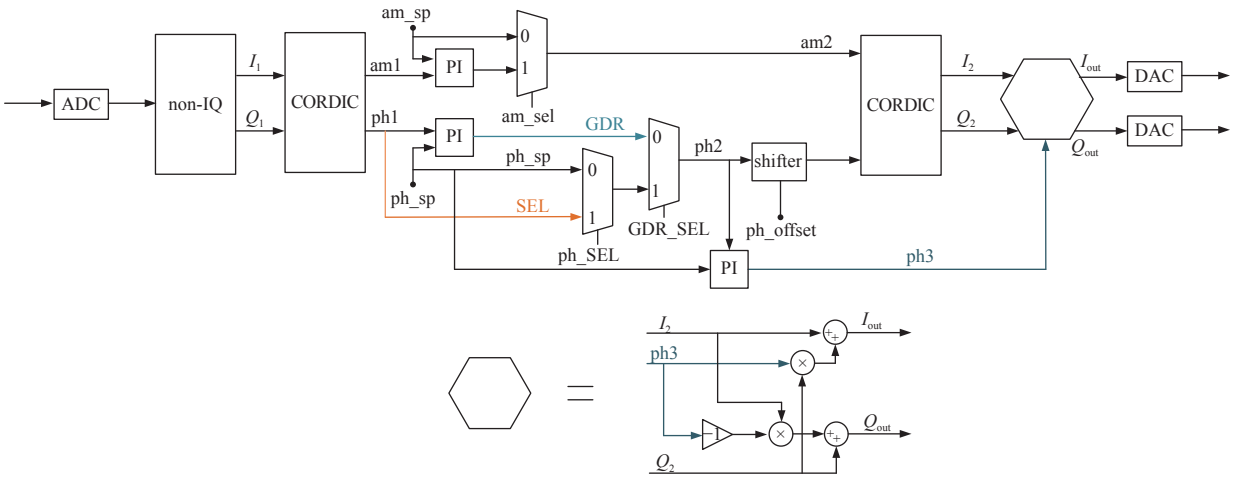

Fig. 3 Structures of the SEL and GDR control algorithm

bandwidths. In the I and Q domains, they perform as sinusoids, while the amplitude remains constant and the phase is up to the detuning frequency of the cavity.

In the locked SEL mode, an additional feedback loop-based phase error is added to the IQ loop. Compared with the CORDIC, the IQ loop decreases the resource and loop delay. The locked SEL mode is developed to compensate for the effects of microphonics detuning of the cavity based on Eq.(5); therefore, it is called a microphonics compensator[20]. Notably, the locked SEL mode is only turned on while the cavity amplitude is kept constant, and the cavity is tuned to approximately the reference frequency.

$$\begin{pmatrix} I_{out} \\ Q_{out} \end{pmatrix} = \begin{pmatrix} 1 & ph_3 \\ -ph_3 & 1 \end{pmatrix} \begin{pmatrix} I_2 \\ Q_2 \end{pmatrix} \tag{5}$$

B. Models in the system generator

The System Generator[21] is a software that can run the data processing algorithm and control system by joining graphical elements from the toolbox and can eventually generate a very high-speed integrated circuit hardware description language (VHDL) or Verilog HDL netlist. Then, the netlist can be downloaded into the FPGA hardware and can efficiently verify the designed algorithm and control system.

The SEL and GDR control systems can be easily built by the add, multiplier, and delay blocks of the system generator. To eliminate the influence of integral saturation in the PI controller, a reset port is placed in the delay block. For the non-IQ algorithm, because the coefficients of the inherent FIR filter in the system generator cannot change with the clock, a moving-average FIR filter is placed with the delay, adder block, and a cycled counter which distribute the in-phase coefficients of the non-IQ to different ADC samples. To the CORDIC block, an inherent CORDIC 5.0 block is added to translate the in-phase and quadrature to the amplitude and phase in the system generator.

In the MicroTCA.4 firmware, the “make file” function can transfer these ports to the register map; thus, they can be arbitrarily read or written.

3 RF Cavity Simulator

The 1.3 GHz 9-cell continuous-wave TESLA type superconducting cavity is used in the SHINE’s main accelerator. The TESLA cavity has 9 passband modes in the frequency domain, which are π/9 2π/9, ⋯ , π. The TESLA cavity operates in the π mode, which is far away from other modes in practice, and the low-level system has bandfilter function, only the π mode can be considered in the simple model analysis. An simplify equivalent π mode LCR circuit can be used to research the characteristics of the RF cavity in the LLRF system.

To build a digital RF cavity model, Ref. [22] gave discrete-I model shown in Eq. (6). However, the discret-I model only perform well in π mode, and also requires a detuning frequency much smaller than the sampling frequency. The detuning frequencies of other modes are likely not satisfied in 1.3 GHz superconducting cavity.

$$\begin{pmatrix} V_{c,i}(n) \\ V_{c,q}(n) \end{pmatrix} = \begin{pmatrix} V_{c,i}(n-1) \\ V_{c,q}(n-1) \end{pmatrix} + \begin{pmatrix} u_{c,i}(n-1) \\ u_{c,q}(n-1) \end{pmatrix} \tag{6}$$

$$A = \begin{pmatrix} 1-T_s\omega_{1/2} & -T_s\Delta\omega \\ T_s\Delta\omega & 1-T_s\Delta\omega \end{pmatrix} \tag{7}$$

$$B = \begin{pmatrix} T_s\omega_{1/2} & 0 \\ 0 & T_s\Delta\omega) \end{pmatrix} \tag{8}$$

Based on the RF cavity baseband mathematics model in the continuous time domain derived by T. Schilcher[22], Ref.[23] built mathematical discrete-II models shown in Eq. (9) in the discrete time domain to implement the cavity model into digital hardware.

$$\begin{pmatrix} V_{c,i}(n) \\ V_{c,q}(n) \end{pmatrix} = C\begin{pmatrix} V_{c,i}(n-1) \\ V_{c,q}(n-1) \end{pmatrix} + D\begin{pmatrix} u_{c,i}(n-1) \\ u_{c,q}(n-1) \end{pmatrix} \tag{9}$$

$$C = \begin{pmatrix} \mathrm{e}^{-T_s\omega_{1/2}}\cos(T_s\Delta\omega) & -\mathrm{e}^{-T_s\omega_{1/2}}\sin(T_s\Delta\omega) \\ \mathrm{e}^{-T_s\omega_{1/2}}\sin(T_s\Delta\omega) & \mathrm{e}^{-T_s\omega_{1/2}}\cos(T_s\Delta\omega) \end{pmatrix} \tag{10}$$

$$D = \begin{pmatrix} 1-\mathrm{e}^{-T_s\omega_{1/2}} & 0 \\ 0 & 1-\mathrm{e}^{-T_s\omega_{1/2}} \end{pmatrix} \tag{11}$$

In our RF cavity simulator, the mathematics model is implemented on boards whose type is the same as the GDR and SEL control systems. Therefore, they can directly connect with each other and afford a real-time platform to test new algorithms of the LLRF control system.

A. The layout of the RF cavity simulator in hardware

Based on the discrete-II model, the cavity model is built in the system generator, as presented in Fig.4, The model also contains amplifiers, limiters, and cavity models. Among them, the amplifier is only a simple linear gain, nonlinear factors can also be added in the future to simulate a more realistic power source output; Limiter rules the maximum power protection system used to simulate the power source so that it does not exceed the normal output range of the power source.

The analog part of the cavity simulator is the same as that of the LLRF system. In Fig.4, only the digital parts of the 1.3 GHz RF cavity simulator are presented. In addition to the non-IQ module, a proportional amplifier, a limiter, and a crucial cavity model are also included in the AMC card.

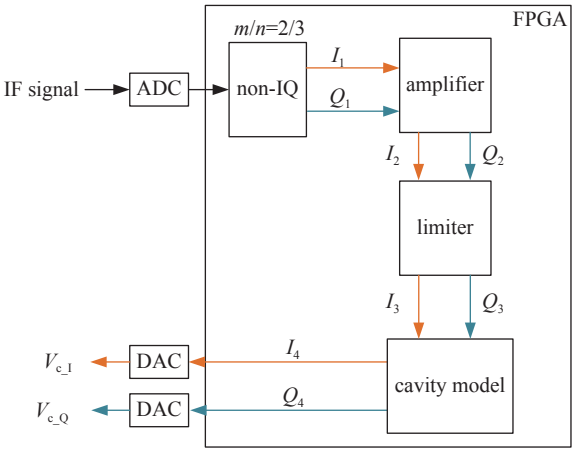

Fig. 4 Layout of the 1.3 GHz cavity simulator

B. The RF cavity model in the system generator

Based on the mathematical model in Eqs.(9)~(11), the RF cavity model is built by adders, multipliers, and delays in the system generator.

To study the appropriate sample bits, this paper compares the continuous model with the bode plots of the 32-bit and 48-bit digit discrete-II model. As shown in Fig.5, the 48-bit model is more accurate and almost overlaps with the continuous model.

4 Implementation and measurements in MicroTCA.4

The hardware of the LLRF system and cavity simulator were installed in the MicroTCA.4 crate. Its cores include the standard AMC SIS8300-L board that provides data processing and I&Q ports, the mRTM DWC8VM1 board which carries mainly analog modules. The MicroTCA.4 crate also has MCH, CPU, SSD, CU, PM, internal clock, trigger distribution, and input/output ports from the rear side, as shown in Fig.6.

To verify the performance of the designed LLRF system, the LLRF system board and the RF cavity simulator are

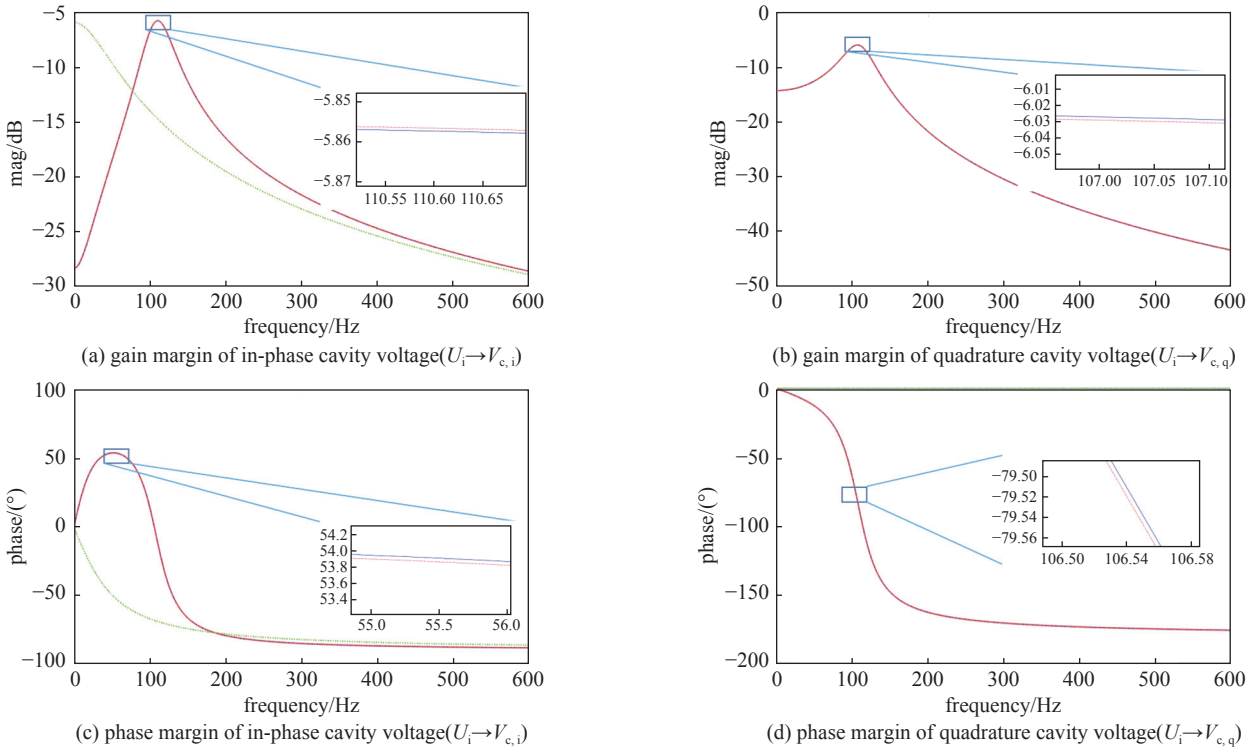

(a) gain margin of in-phase cavity voltage($U_i \rightarrow V_{c,i}$)

(b) gain margin of quadrature cavity voltage($U_i \rightarrow V_{c,q}$)

(c) phase margin of in-phase cavity voltage($U_i \rightarrow V_{c,i}$)

(d) phase margin of quadrature cavity voltage($U_i \rightarrow V_{c,q}$)

Fig. 5 Comparison of bode plots with different bit lengths of the 1.3 GHz continuous wave superconducting cavity digital model (blue line: continuous model; green line: 32 bit; red line: 48 bit)

connected to each other from the rear IO ports through RF coaxial cables. The data of different parts in the LLRF and cavity simulator can be picked up and transported to the CPU and SSD using the MicroTCA.4 firmware.

Fig.7 is the diagram of address space and interfaces connection of MicroTCA.4 firmware. All of them deliver date to other board or outside by board interconnect and peripheral component interface express (PCIe), and they are implemented in FPGA chips. All boards use the same backplane and have the same zone3 or FPGA mezzanine card (FMC) connectors. In each board, the data are processed by CPU over PCIe and send to other boards over multi-gigabit transceivers (MGT).

In the interface connection, the internal memory access bus (IBUS) always connect with communication interface and is used to contact registers and memory in FPGA with CPU. The data acquisition bus (DAQ) can read out the data streams from FPGA to external memory by first-in first-out (FIFO) buffers. The direct memory access (DMA) is used to access the data over communication interface. Low latency links bus (LLL) is responsible for point to point communication between AMC boards by MGT[24].

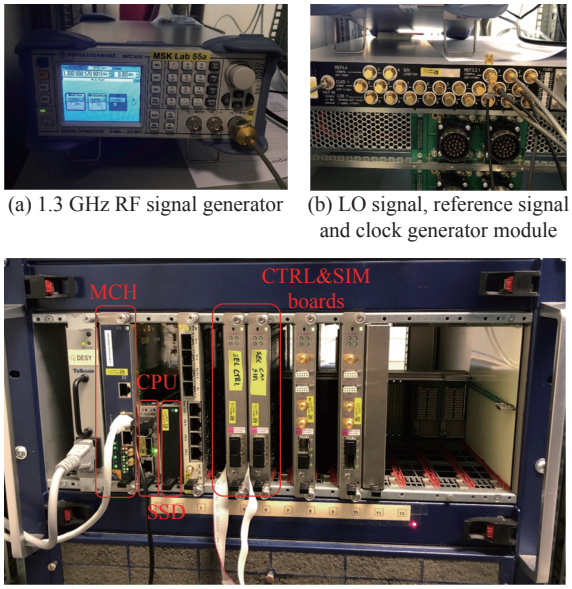

(a) 1.3 GHz RF signal generator

(b) LO signal, reference signal and clock generator module

(c) MicroTCA.4 crate

Fig. 6 Hardware of the LLRF system and cavity simulator

According to the RF cavity bode plot and phase shift shown in Eq.(12)[11], we can obtain the theoretical value of amplitude and phase shift when the RF cavity is detuning.

$$\tan\phi = 2Q_L\frac{\Delta f}{f_0} \tag{12}$$

To validate the cavity simulator, a constant normalized step signal is input, and the data of V_{c_I} and V_{c_Q} are acquired and

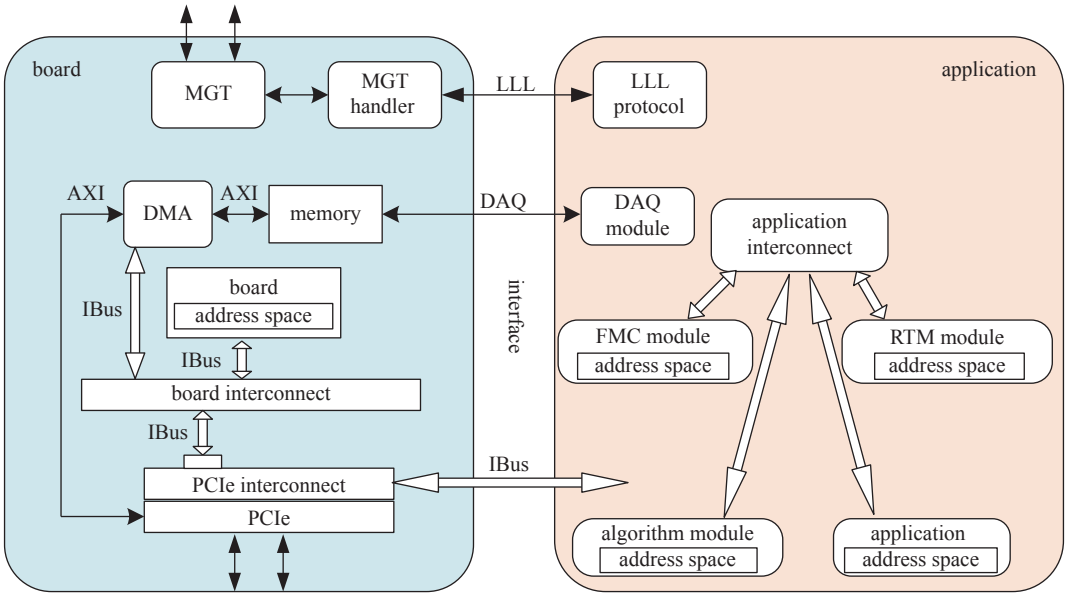

Fig. 7 Diagram of address space and interfaces connection of MicroTCA.4 firmware[23]

converted to amplitude and phase values. The measured values and ideal values of the cavity field under the cavity simulator detuned at 50 Hz is present in Fig.8. The average amplitude and phases deviations between the ideal and measured values measured for several times are $\Delta V_c/V_c \times 100\% \approx 0.05\%$ and $\Delta\phi \approx 3\times10^{-3}(^\circ)$. Because the cavity mathematical model performs similar to a low-pass filter in the frequency domain, the measured values form a straight line.

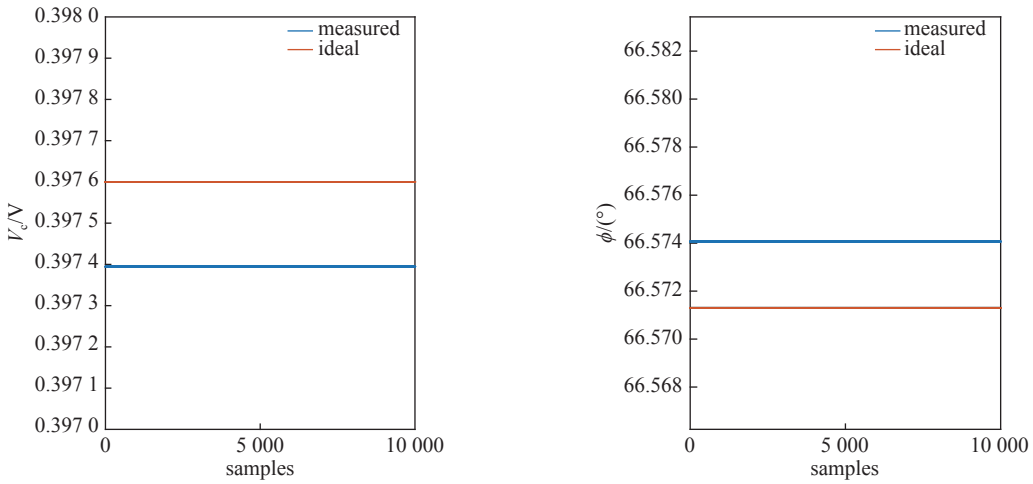

(a) amplitude of the cavity field (b) phase of the cavity field

Fig. 8 Measured values and ideal values of the cavity field under the cavity simulator detuned at 50 Hz

In the GDR mode, the selector of GDR_SEL is set to 0, and the amplitude loop selector is 1. The gains of the microphonics compensator need to be zero. After the gains of the phase feedback loop and amplitude feedback loop are adjusted properly, a constant cavity field can be easily maintained. If the cavity simulator is detuned several bandwidths, the amplitude and phase of the cavity field will be unstable.

To test the SEL mode, the cavity simulator was detuned at 5 Hz. The gains of the PI in the microphonics compensator were set to zero, the GDR_SEL was set to 1, and the amplitude loop could switch to the PI feedback loop. The testing results are shown in Fig.9. Note that the $V_{\text{c-am}}$, $V_{\text{c-ph}}$, I_{out}, Q_{out} in Fig.9 correspond to am1, ph1, I_{out}, Q_{out} in the Fig.3, respectively. The results show that the SEL loop performs similar to a PLL system owing to the drawbacks of the inherent CORDIC block of the system generator. The phase shifter of the SEL loop can offset the loop phase shift caused by the detuning cavity. The amplitude of the cavity field is stable and unaffected by the ponderomotive instabilities. Due to the marginally detuned RF cavity and the invariable frequency of the RF power source, the amplitude response of the cavity field in detuning cavity will be

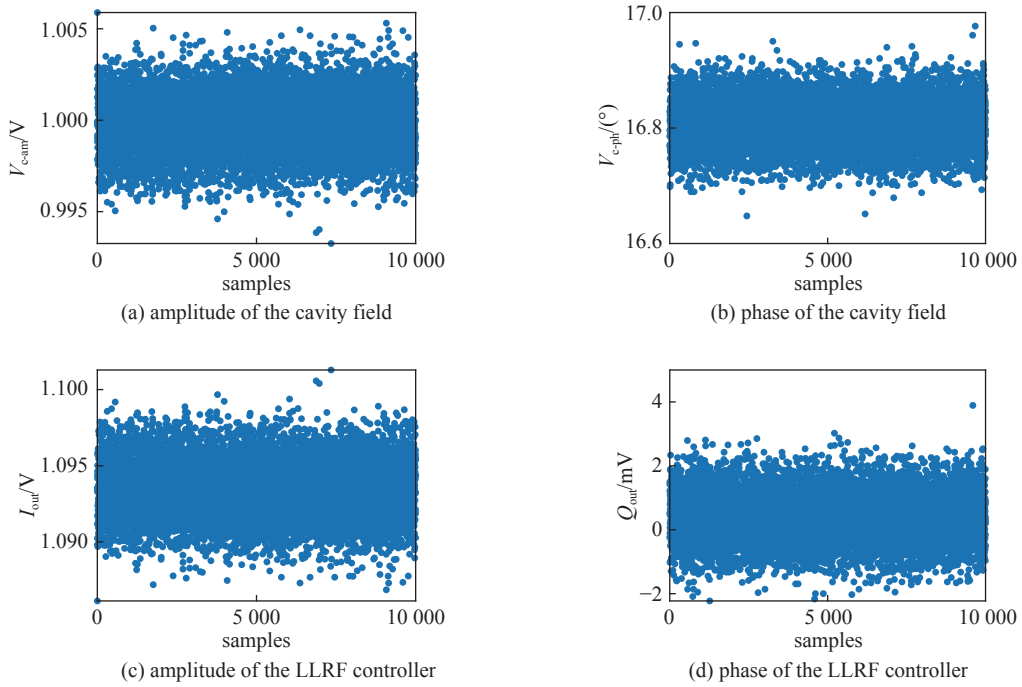

(a) amplitude of the cavity field

(b) phase of the cavity field

(c) amplitude of the LLRF controller

(d) phase of the LLRF controller

Fig. 9 Amplitude and phase of the cavity field and the output of the LLRF controller in the locked SEL mode when the detuning frequency is 5 Hz

lower than in the resonant cavity. To keep the amplitude of the cavity filed to the set-point, the amplitude feedback make the output of I component in the LLRF controller slightly more than 1. The amplitude feedback loop regulates the amplitude of the cavity field to the set point, and the stability of the amplitude of the cavity field is 0.454 8% (RMS).

5 Conclusion

A digital LLRF control system for a 1.3 GHz CW-operated RF cavity was designed and developed in this study. The LLRF control system has three operation modes. The GDR mode is suitable for operating in the cavity, and the resonant frequency is approximately equal to the reference frequency. The free SEL mode can track the cavity frequency and is suitable for operating in the detuned cavity. The locked SEL mode is used to compensate for the effects of microphonics. In this study, the system generator was applied to quickly realize and verify the new LLRF control system or algorithms. A digital cavity simulator was also developed and implemented to decrease the risk of cavity damage during the testing process and easily test the performance of advanced LLRF system algorithms.

The measurement results of the cavity simulator and the digital LLRF system in MicroTCA.4 are presented in Section 4. This demonstrates that the cavity simulator performs well and has adequate ability to test new algorithms of the LLRF system. The locked SEL can automatically compensate for cavity detuning and maintain the amplitude and phase close to the reference values. In the future, a more efficient and accurate CORDIC block will be designed and developed. The cavity simulator will also include the effects of Lorentz force detuning, beam loading, and microphonics to achieve a more realistic simulation of the RF cavity.

Acknowledgement The authors gratefully acknowledge Lukasz Butkowski for his guidance and assistance with the system generator and MicroTCA.4 and are sincerely thankful to Julien Branlard, Cagil Gümüs, Michael Burkart, Burak Dursun, and Holger Schlarb for their support and helpful discussions during a one-year stay in DESY.

References:

[1] Rolles D. Time-resolved experiments on gas-phase atoms and molecules with XUV and X-ray free-electron lasers[J]. Advances in Physics: X, 2023, 8: 2132182.

[2] McNeil B W J, Thompson N R. X-ray free-electron lasers[J]. Nature Photonics, 2010, 4(12): 814-821.

[3] Liu Tao, Huang Nanshun, Yang Hanxiang, et al. Status and future of the soft X-ray free-electron laser beamline at the SHINE[J]. Frontiers in Physics, 2023, 11: 1172368.

[4] Liu Kui, Li Lin, Wang Cheng, et al. Multi-port cavity model and low-level RF systems design for VHF gun[J]. Nuclear Science and Techniques, 2020, 31: 8.
[5] Neumann A. Compensating microphonics in SRF cavities to ensure beam stability for future free electron lasers[D]. Hamburg: University of Hamburg, 2008.
[6] Neumann A, Anders W, Kugeler O, et al. Analysis and active compensation of microphonics in continuous wave narrow-bandwidth superconducting cavities[J]. Physical Review Special Topics-Accelerators and Beams, 2010, 13: 082001.
[7] Luo Lei, Sun Jinwei, Huang Boyan. A novel feedback active noise control for broadband chaotic noise and random noise[J]. Applied Acoustics, 2017, 116: 229-237.
[8] Badillo I, Jugo J, Portilla J, et al. Pxie-based LLRF architecture and versatile test bench for heavy ion linear acceleration[J]. IEEE Transactions on Nuclear Science, 2015, 62(3): 963-971.
[9] Reece C. Overview of SRF-related activities at Jefferson Lab[C]//Proceedings of the 10th Workshop on RF Superconductivity. 2001.
[10] Schulze D. Ponderomotive stability of R. F. resonators and resonator control systems[R]. ANL-TRANS-944, 1972.
[11] Delayen J R. Phase and amplitude stabilization of superconducting resonators[D]. California: California Institute of Technology, 1978.
[12] Pławski T. Digital RF control system for superconducting cavity with large Lorentz force detuning coefficient[D]. Warsaw: Warsaw University of Technology, 2014.
[13] Konrad M. Development and commissioning of a digital rf control system for the S-DALINAC and migration of the accelerator control system to an EPICS-based system[D]. Darmstadt: Technische Universität Darmstadt, 2013.
[14] Powers T. Practical aspects of SRF cavity testing and operations[C]//SRF Workshop. 2011: 60-63.
[15] Geßler P. Synchronization and sequencing of data acquisition and control electronics at the European X-ray free electron laser[D]. Hamburg: Technische Universität Hamburg, 2015.
[16] Doolittle L, Ma Hengjie, Champion M S. Digital low-level RF control using non-IQ sampling[C]//Proceedings of LINAC2006. 2006: 568-570.
[17] Geng Zheqiao, Kalt R. Advanced topics on RF amplitude and phase detection for low-level RF systems[J]. Nuclear Science and Techniques, 2019, 30: 146.
[18] Li Xiao, Sun Hong, Long Wei, et al. Design and performance of the LLRF system for CSNS/RCS[J]. Chinese Physics C, 2015, 39: 027002.
[19] Du Botao, Lin Hongxiang, Liu Wei, et al. DSP Frame and Algorithm of LLRF of IR-FEL[C]//Proceedings of IPAC2017. 2017: 4017-4019.
[20] Andraka R. A survey of CORDIC algorithms for FPGA based computers[C]//Proceedings of the 1998 ACM/SIGDA Sixth International Symposium on Field Programmable Gate Arrays. 1998: 191-200.
[21] Mittal S, Gupta S, Dasgupta S. System generator: the state-of-art FPGA design tool for DSP applications[C]//Third International Innovative Conference on Embedded Systems, Mobile Communication and Computing (ICEMC2 2008). 2008: 187-190.
[22] Schilcher T. Vector sum control of pulsed accelerating fields in Lorentz forces detuned superconducting cavities[D]. Hamburg: University of Hamburg, 1998.
[23] Qiu Feng, Michizono S, Miura T, et al. Application of disturbance observer-based control in low level radio-frequency system in a compact energy recovery linac at KEK[J]. Physical Review Special Topics-Accelerators and Beams, 2015, 18: 092801.
[24] Butkowski L, Kozak T, Yang Bin, et al. FPGA firmware framework for MTCA. 4 AMC modules[C]//Proceedings of the 15th International Conference on Accelerator and Large Experimental Physics Control Systems. 2015.

1.3 GHz 连续波超导射频腔的数字低电平射频系统和腔模拟器设计及测试

刘 奎[1,2], 王 程[3], 黄宇轩[1,2], 朱坤托[1,2], 王 滔[1,2]

(1. 上海航天智能计算技术重点实验室, 上海 201109; 2. 上海航天电子技术研究所, 上海 201109;
3. 中国科学院 上海高等研究院, 上海 201210)

摘 要: 1.3 GHz 连续波超导射频腔需要高精度低电平射频(LLRF)系统来稳定超导腔的电磁场。但由于 1.3 GHz CW 射频腔的高负载品质因数和宽电磁频段,射频腔在频域中的电磁带宽较小。射频功率源与射频腔体之间的微小电磁频率差异易造成发生器驱动谐振器控制系统的不稳定,最终导致腔体电磁场的变化。开发了一种自激环控制系统,以防止“有质”不稳定性的发生,并补偿微噪声的影响。此外,还开发了数字 1.3 GHz 射频腔体模拟器,用于验证 LLRF 系统的设计算法。测试表明,即使在射频腔失谐 5 Hz 时,自激励控制系统也能确保腔场的稳定性。经过对比,验证了 1.3 GHz 射频腔体模拟器是测试新算法的可靠平台。

关 键 词: RF 腔模拟器; 自激励环路; 发生器驱动; RF 低电平控制系统